ELSEVIER

Tectonophysics 258 (1996) 35–51

TECTONOPHYSICS

Rupture history and seismotectonics of the 1991 Uttarkashi, Himalaya earthquake

F. Cotton [a,*], M. Campillo [a], A. Deschamps [b], B.K. Rastogi [c]

[a] *Laboratoire de Géophysique Interne et de Tectonophysique (URA CNRS 733), Université Joseph Fourier, IRIGM BP 53X. F38041, Grenoble Cedex, France*

[b] *Institut de Géodynamique, CNRS-Sophia Antipolis 06560, Valbonne, France*

[c] *National Geophysical Research Institute, Hyberabad, 500007, India*

Received 22 November 1994; accepted 16 October 1995

Abstract

The 19 October 1991 Uttarkashi, India earthquake occurred in the main thrust zone of the Himalaya. With a moment magnitude of 6.8, this event is characteristic of the present-day motion on the thrust fault system. We examine this earthquake using different sets of data in order to understand better the faulting process of a major earthquake in the Himalayan region. Firstly, the modeling of the teleseismic records indicates that the mechanism is similar to the published CMT and indicates a shallow (between 10 and 15 km depth) low-angle thrust event. In the vicinity of the source, the earthquake was recorded by a network of accelerometers run by the University of Roorkee. Six three-component accelerometers were triggered within a radius of 60 km. Two of them were very close to the surface projection of the fault. Forward modeling of those records shows that the rupture propagated toward the west. This forward modeling gives us the possibility to confirm the epicenter location and to evaluate the timing of the accelerograms. The accelerogram records are inverted to obtain the distribution of slip on the fault plane. The results show a complex rupture process. The slip maxima (1.5 m) occurred 10 km west and 15 km southwest of the hypocenter. The slip source function obtained with near-field data is similar to the function obtained from teleseismic records and shows a low moment release at the beginning of the rupture and a maximum rate of moment release 4 seconds after. The relation between the slip distribution obtained by inversion, isoseimals, mapped faults and the aftershocks location is then discussed and we finally propose a seismotectonic interpretation of this earthquake. The Uttarkashi earthquake probably occurred along the detachment surface which coincides with the upper surface of the subducting Indian lithosphere. This detachment surface is gently dipping under the Lesser Himalaya and south of the Vaikrita thrust. The Vaikrita thrust marks the line separating the very shallow-dipping detachment (along which big earthquakes like the Uttarkashi earthquake could occur) from the steeper-dipping, aseismic basement thrust. This observation is important for correctly estimating the seismic hazard in the Uttarkashi region.

1. Introduction

The 20 October 1991 Uttarkashi earthquake (M_s = 7.0) killed over a thousand people and caused important economic loss in the Garhwal, Himalaya region. The earthquake occurred in the Himalaya mountains (India) at the plate boundary between the colliding Indian and Asian plates. The earthquake also generated a great deal of interest because it is located within a distance of 50 km from the site of the Tehri dam under construction to the south. In the

* Corresponding author.

SSDI 0040-1951(95)00154-9

Garhwal region, several earthquakes are known to have occurred in historical times (Rastogi, 1994). The most important one, the event of 1803 with intensity IX, was highly destructive (Smith, 1843). The study of this 1991 earthquake is then important for the assessment of hazards in this region and more generally in seismically active collision environments.

This earthquake is the largest well-recorded earthquake in the Himalaya to date. We examine this earthquake using all available types of seimological data (aftershocks, teleseismic, strong-motion records) in order to understand better the faulting process in the Himalayan collision environment. In a first step, we have used a waveform inversion of teleseismic data to obtain the focal mechanism and the time history of moment release of the Uttarkashi earthquake. This earthquake had also the unique chance to be recorded by a network of accelerometers in the near field. These strong-motion records represent the most complete set of accelerograms for a thrust earthquake in the Himalayan region (Chandrasekaran and Das, 1992). Methods for estimating slip distributions and rupture characteristics using waveform inversions of near-source seismograms have been also developed and applied to many earthquakes in California (Olson and Apsel, 1982; Hartzell and Heaton, 1983; Beroza and Spudich, 1988; Cohee and Beroza, 1994; Wald and Heaton, 1994; Cotton and Campillo, 1995), in subduction (Fukuyama and Irikura, 1986; Takeo, 1987; Mendoza et al., 1994) and intraplate zones (Hartzell and Mendoza, 1991) but never in a collisional tectonic context like the Himalayan orogen. These strong-motion records give us the opportunity to apply a newly developed, deterministic, inversion technique (Cotton and Campillo, 1994, 1995) to a major thrust Himalayan earthquake.

This event is characteristic of the tectonic processes currently affecting the Garhwal province. It provides information on the present-day motion on the thrust fault system and the relative roles of the different faults in accomodating the plate tectonic motion. In this paper, we examine the relationship between the differents faults, the main shock and the aftershocks of the Uttarkashi earthquake.

2. Seismotectonic setting

The Uttarkashi forms the plate boundary between the Indian and the Asian plates. From the pioneering work of Argand (1924), numerous authors discussed the collision between these two plates and the formation of the Himalaya (for example: Gansser, 1964;

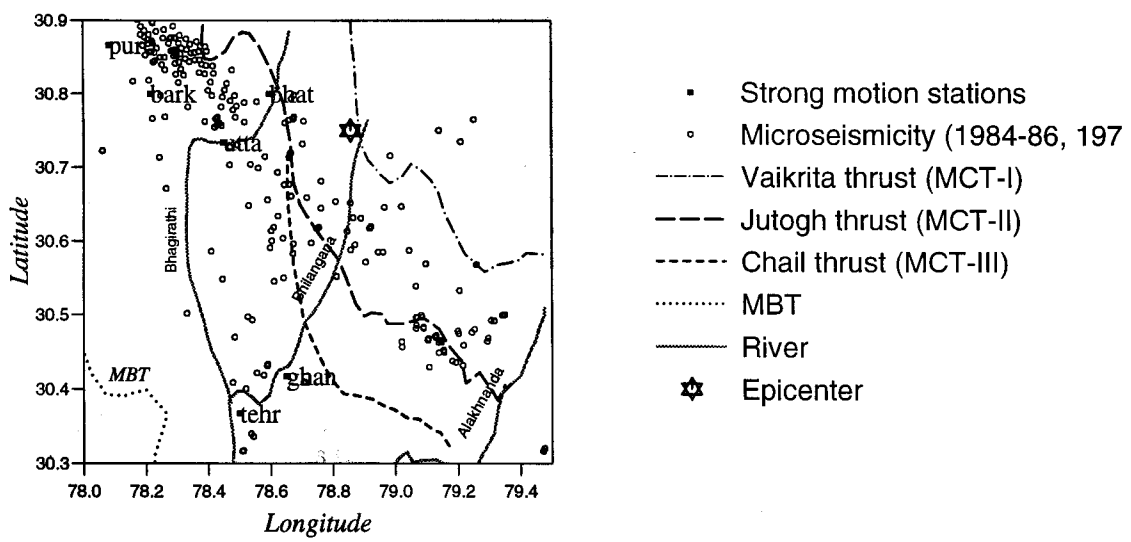

Fig. 1. Map of the Uttarkashi region showing the strong-motion stations used in this study, the main thrusts of this region and the microseismicity recorded by the University of Roorkee in 1984–1986 and 1979–1980.

Molnar and Tapponier, 1975; Tapponnier and Molnar, 1977; LeFort, 1975; Seeber et al., 1981; Lyon-Caen and Molnar, 1983; Ni and Baranzangi, 1984). The total convergence between India and Asia has been estimated to be about 2000–3000 km. About 300–500 km could have occurred along the Himalaya by repeated overthrusting of Indian crust on itself. These thrusts separate geological units with characteristic geology (Gansser, 1964). The southernmost unit, named the outer Himalaya, consists of the folded and faulted Siwalik molasse sediments of Miocene age. These molasse sediments form the low hills that rise in front of the plains of the Sindhu–Ganga basin. The Outer Himalaya is separated from the Lesser Himalaya in the north by the Main Boundary Thrust (MBT). The most northerly subprovince is the Great Himalaya which is made up of crystalline metamorphic and igneous rocks. The slab of the great Himalaya is thrusting southward along the Main Central Thrust (MCT) over the Lesser Himalaya. In the Uttarkashi region, the problem is more complex because it is difficult to locate precisely the MCT. There are three major sets of northward-dipping thrusts which are called, from north to south the Vaikrita Thrust (MCT-I), the Jutogh Thrust (MCT-II) and the Chail Thrust (MCT-III) (Fig. 1). The inclination of these thrust planes varies between 30 and 40° (Valdiya, 1980). Seeber et al. (1981) postulated a gently dipping thrust under the Lesser Himalaya. They called this plane the detachment surface which coincides with the upper surface of the subducting Indian lithosphere. The MBT and MCT which dip steeply (30–40°) near the surface flatten out at depth and merge with this surface. Downdip from the interplate thrust zone the detachment presumably becomes steeper and eventually bends back to merge with a subhorizontal aseismic interplate zone beneath the northern Tethyan Himalaya and Tibet.

The distribution of seismicity throughout the Himalaya appears to form a belt of moderate-sized events ($m_b < 6$) beneath the Lesser Himalaya between the MCT and the MBT (Molnar et al., 1973; Chandra, 1978; Seeber et al., 1981; Ni and Baranzangi, 1984). Most of those events are located just south of the MCT. Medium-sized earthquakes with fault plane solutions and well-determined focal depths determined by Ni and Baranzangi (1984) define a simple planar zone from about 10 to 20 km depth, with an apparent dip of 15°. This planar zone apparently defines the detachment that separates the underthrusting Indian plate from the Lesser Himalaya crustal block and along which, according to Seeber et al. (1981) and Ni and Baranzangi (1984) occurred the great Himalayan earthquakes which have struck the Himalayan arc during the past 90 years. Four magnitude-8 earthquake have occurred since 1897 on the Himalaya plate boundary. The Uttarkashi earthquake occurred near the northwestern part of a seismic gap called the Central gap by Khattri (1987).

3. Study of the rupture using teleseismic data

The use of full waveform modeling of long-period teleseismic data has improved our knowledge of the rupture process of large earthquakes with teleseismic data (Nábèlek, 1985; Mendoza and Hartzell, 1989; Campos et al., 1994). In a first step, we have used a full waveform inversion of teleseismic data to determine the focal mechanism and the time history of moment release of the Uttarkashi earthquake. We have selected 34 broad-band body wave (22 P and 12 S) records from IRIS/GSN, MEDNET and GEOSCOPE networks to obtain the seismic moment tensor, the mean focal depth and the general features of the source in time as seen from distant stations. The station distribution at distance range from 30 to 80° is good (Table 1; Fig. 2). Since the VBB coverage is poor in the lower hemisphere, we are required to consider together BRB and VBB stations. All the records are numerically converted to the same response curve and displacements are inverted in the frequency range of 0.02 to 2 Hz. The procedure proposed by Nábèlek (1984) is used in the inversion. This procedure allows a multiple source inversion and solves simultaneously for focal mechanism, centroïd depth and source time function. The first inversion was performed assuming a single point source associated with a single mechanism and a source duration of 14 s composed of 2 s elementary triangle sources. The results gives a good fit to the data with a centroid depth of 14 km, a global seismic moment of 1.2 10^{19} N m, a strike of 318°, a dip of 11° and a rake of 114°. The source time function (Fig. 3) shows three sharp subevents with a total duration of

Table 1
Stations used in the body-wave teleseismic inversion

Code	Institution [a]	Type	Azimut	Distance	Used wave
ALE	IRIS	VBB	354.8	65.4	P, S
AQU	MEDNET	VBB	302.0	52.6	P
BGY	MEDNET	VBB	304.4	47.2	P
BJI	CDSN	BRB	62.5	31.6	P, S
BNI	MEDNET	VBB	306.4	56.9	P, S
COL	GSN/USGS	VBB	18.5	78.0	P, S
CRZF	GEOSCOPE	BRB	198.5	80.6	P
ERM	IRIS	VBB	18.5	78.0	P, S
ESK	IRIS	VBB	319.6	60.9	P, S
GUMO	GSN	VBB	90.0	62.7	P
HIA	CDSN	BRB	47.1	35.9	P
INU	GEOSCOPE	VBB	68.3	48.4	P, S
KEG	MEDNET	VBB	281.2	40.3	P
KEV	DWWSSN	VBB	338.6	48.5	P, S
KIV	IRIS	VBB	305.1	31.3	P
KONO	GSN	VBB	323.9	53.6	P
OBN	IRIS	VBB	321.7	38.5	P, S
PAF	GEOSCOPE	BRB	185.7	80.1	P
RER	GEOSCOPE	VBB	206.1	56.1	P, S
TAM	GEOSCOPE	VBB	164.9	66.0	P, S
TOL	GSN	VBB	303.3	66.0	P, S
VSL	MEDNET	VBB	299.3	56.2	P

Type of record concerns the frequency band: VBB, 0.005–10 Hz; BRB, 0.06–2 Hz.
[a] CDSN = Chine Digital Seismograph Network; GDSN = Global Digital Seismograph Network; GSN = Global Seismographic Network; GEOSCOPE = Project Geoscope; IRIS = Inorporated Research Institutions for Seismology; MEDNET = Mediterranean Network.

8 s. A small precursor could be observed on seismograms at stations where the signal to noise ratio is low like stations HIA and BJI, but is not determined by the inversion procedure. The results clearly show a complex source time. The main seismic moment release occurred after an initial pulse of 2 s duration. The source function of this main event shows three sharp subevents of a total duration of 8 s. The comparison between observed and calculated seismograms in displacement is quite good in the initial part of the signal and deteriorates later when crustal reverberations appear that are not taken into account in our modeling.

We tried in a second step to determine a source directivity, assuming that the three different parts of the source are associated with different point sources,

Table 2
Focal parameters of the Uttarkashi earthquake

Source	Localization	Moment ($\times 10^{19}$ N m)		Strike (°)	Dip (°)	Rake (°)	Depth (km)
IMD [a]	30.75°N						12.0
	78.86°E						
CMT	30.22°N	1.8	NP1	317	14	115	15.0
(Harvard)	78.24°E		NP2	112	78	84	
USGS	30.78°N	1.8	NP1	296	5	90	10.0
	78.77°E		NP2	116	85	90	
This study		1.2		318	11.0	114	14.0

[a] India Meteorological Department.

with slightly different mechanisms along the N318° direction. The resolution of the teleseismic data for such details is poor, and none of our results was convincing enough to imply more on the source mechanism process with this data set.

The results obtained for the focal mecanism are quite comparable to those obtained by other teleseismic analyses (Table 2). These teleseismic inversions give values of the moment between 1.2×10^{19} N m (our study) and 1.8×10^{19} N m (CMT determination).

4. Study of the rupture using strong-motion data

4.1. Data

Thirteen SMA-1 strong-motion instruments were triggered by the Uttarkashi earthquake in the distance range of 25–150 km. Among these thirteen stations, six are close enough to have sufficient amplitude to be usable in the waveform inversion (Table 3). Each of those stations recorded three components of ground acceleration and the three

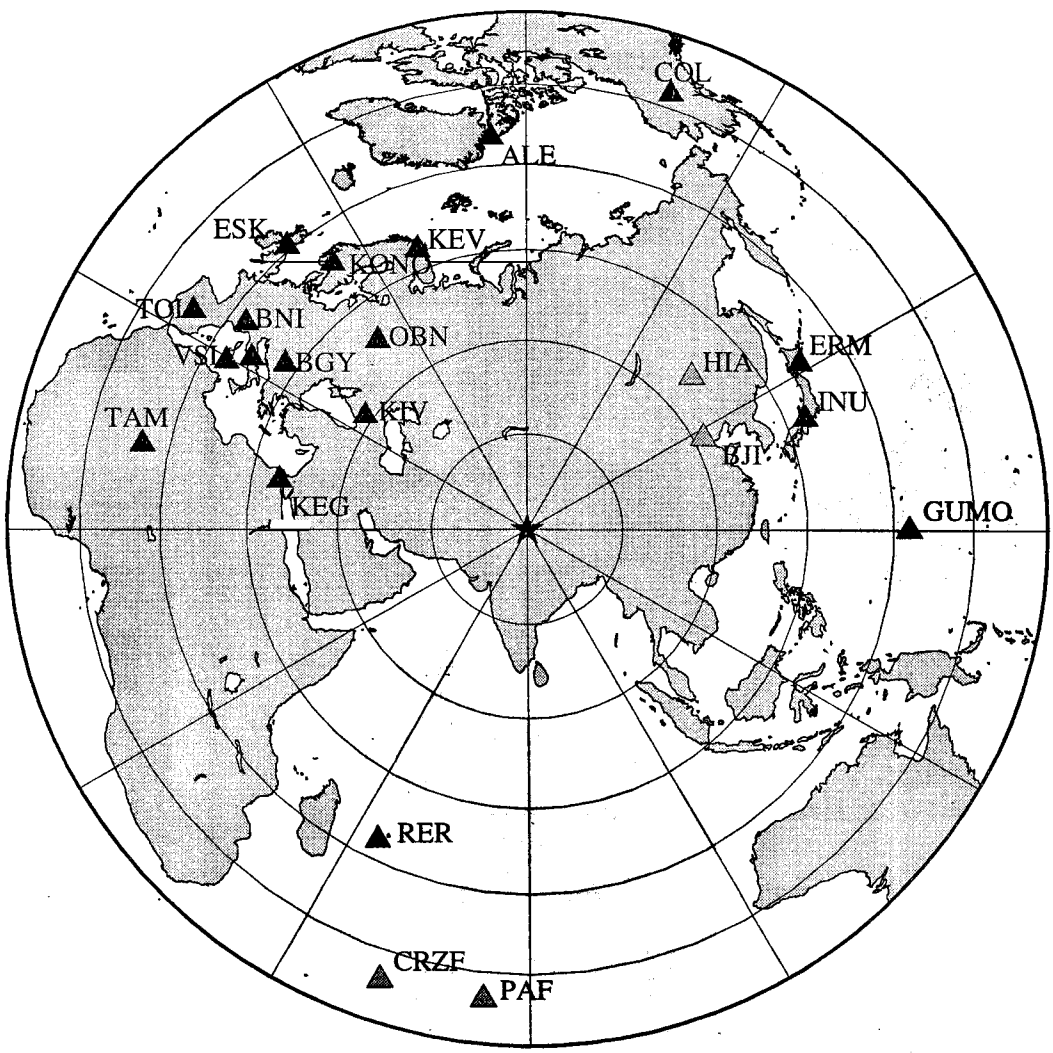

Fig. 2. Azimuthal coverage of the source around the epicenter (★ in the center) by the broad-band digital stations used in this study. ▲ are for VBB records, △ for BRB records.

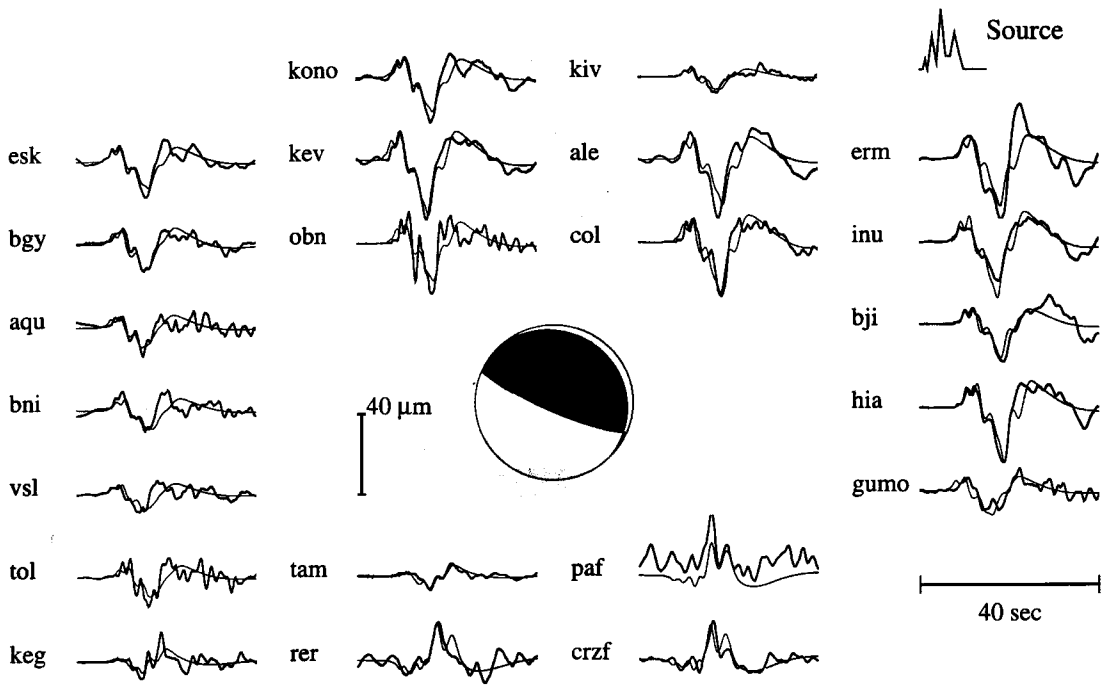

Fig. 3. Comparison of observed P-wave records (thick line) in displacement and synthetic seismograms (fine line) for the best point source model of the 1991 Uttarkashi earthquake found by our teleseismic body-wave inversion. All of them are filtered between 0.02 and 2 Hz, normalized to a recording distance of 40° and plotted at the same amplitude scale. The focal mechanism (strike = 318°, dip = 11°, rake = 114°, depth = 14 km, seismic moment = 1.2 10^{19} N m) and the source–time function of this model are shown in the middle and the right top of the figure.

components were used in this study. Because of the difficulty in modeling high frequencies the acceleration records have been band-passed filtered from 0.17 to 0.6 Hz. The filtering is done to remove frequencies outside the bandwidth for which Green's functions could be accurately evaluated. In this frequency band, the latest part of the signal is made up of low-velocity surface waves that propagate in the shallow layers. These late arrivals do not give information on the rupture process and can not be modeled in a simple plane layered crustal model. The information on the rupture process is given by the first P and S waves that have energy in a large frequency band. Therefore, to eliminate the low-frequency late arrivals, the traces filtered between 0.1 and 0.6 Hz have been multiplied by the normalized envelopes of the signal filtered between 0.1 and 5.0 Hz in order to select the body wave part of the signals.

Table 3
Stations used in the strong-motion inversion

Stations	Code	Latitude	Longitude
Barkot	bark	30°48′N	78°13′E
Bhatwari	bhat	30°48′N	78°35′E
Ghansiali	ghan	30°25′N	78°39′E
Purola	puro	30°52′N	78°05′E
Tehri	tehr	30°22′N	78°30′E
Uttarkashi	utta	30°44′N	78°27′E

4.2. Forward modeling of strong ground motion

The details of the method used have been presented by Cotton and Campillo (1994, 1995). Here we introduce this method briefly. In this procedure, we divide the fault plane into small rectangular regions of equal area called subfaults. Each subfault is allowed to slip once. With this parameterization,

the ground motion (V) at a given station i and a given frequency ω can be represented as a linear sum of n subfault contributions, each appropriately delayed in time to account for front propagation:

$$V_i(\omega) = \sum_{k=1}^{n} \text{slip}(k) \exp^{-i\omega t(k)} u_{ki}(\omega) S_k\left[R_{(k)}, \omega\right] \quad (1)$$

where U_{ki} represents the ground motion for a unit constant slip on the subfault k with a given source mechanism and ω is the angular frequency. Slip(k), $t(k)$ and S_k are the final slip, the rupture time and the source function of the kth subfault depending on a single variable: the rise time $R(k)$. This simple parameterization allows to limit the number of parameters of the model with respect to the technique proposed by Olson and Anderson (1988).

From a practical point of view, each subfault is represented by an array of point sources separated by a distance of less than one sixth of the shortest wavelength. The subfault contributions U_{ki} are obtained by summing the response of these point sources appropriately delayed in time to include the travel-time difference due to the propagation of the rupture front across each subfault. A local rupture velocity is therefore assumed for the integration on a subfault. The point-source Green functions are calculated for a layered velocity model using the discrete wavenumber integration method (Bouchon, 1981) associated with the reflection transmission matrix method (Kennett, 1983). In this study we used the regional seismic model (Table 4) given by Khattri (1992). We expect that site effects are of limited importance in the frequency band of our study. Therefore given a layered crustal model and assuming on each subfault a constant focal mechanism and a local rupture velocity, $V_i(\omega)$ can be considered as a function of slip(k), $t(k)$ and $R(k)$.

4.3. Inverse modeling of strong ground motion

The parameter vector p and data vector d are related by the function model vector f as $d = f(p)$. In the case of the Uttarkashi earthquake, the number of data (six stations) is much lower than the number of stations used in previous inversions with the same technique, such as the inversion of the 1992, Landers earthquake (eleven stations, Cotton and Campillo, 1995). For this reason, we have chosen to restrain the number of parameters describing the Uttarkashi earthquake. In the following inversions, slip is constrained to be positive, and the rise time is constant on all the subfaults. The parameters of the inversion are slip(k) and $t(k)$ which appear in Eq. (1). Slip(k) is by definition positive, so taking a gaussian function to model the a priori information is not appropriate because a gaussian function gives a non-null probability to negative values. To avoid this problem, we choose to inverse the logarithm of this parameter, which defines a new (unbounded) parameter whose a priori density is gaussian and for which our standard inversion technique applies (Tarantola, 1987). The elements of d consists of complex three-component spectra from all stations. The f function is a non-linear function of $t(k)$ and $R(k)$. If we assume an initial parameter vector p_0, we can get the iterative solution p_k by linearization of f around p_0 at the first iteration and around p_{k-1} at each subsequent iteration k. Using the observed data vector d_0 and an inversion algorithm based on the work by Tarantola and Valette (1982), p_{k+1} is given by:

$$p_{k+1} = p_k + b\left(A_k^t C_d^{-1} A_k + C_p^{-1}\right)^{-1} \times \left\{A_k^t C_d^{-1}\left[d_0 - f(p_k)\right] + C_p^{-1}(p_0 - p_k)\right\} \quad (2)$$

Here A_k is the Jacobian matrix of $f(p_k)$ (the ijth

Table 4
Reference regional velocity model

Thickness (km)	V_p (km/s)	V_s (km/s)	Density (g/cm^3)	Q_p	Q_s
0.4	3.5	2.00	1.80	50.0	25.0
1.0	5.0	2.86	2.40	80.0	50.0
15.0	5.2	2.97	2.60	4000.0	2000.0
30.0	6.0	3.43	2.90	4000.0	2000.0
∞	8.33	4.83	3.30	100.0	500.0

element of A_k is $[\partial f_i(p_k)]/[\partial(p_k)_j]$, b is a damping constant between 0 and 1 used to prevent divergence, and C_p and C_d are the covariance matrices for p and d. Because a functional form of the slip is assumed, all derivatives are evaluated analytically.

The fit to the data at each iteration k is evaluated using the misfit function S (Tarantola and Valette, 1982):

$$S(p_k) = \tfrac{1}{2}\Big\{[f(p_k)d_0]^t C_d^{-1}[f(p_k) - d_0] + (p_k - p_0)^t C_p^{-1}(p_k - p_0)\Big\} \quad (3)$$

Following Cohee and Beroza (1994), we also evaluate the variance reduction between theoretical and observed seismograms defined as:

$$\Delta\sigma^2 = 1 - \frac{[d_0 - f(p_\infty)]^t C_d^{-1}[d_0 - f(p_\infty)]}{d_0^t C_d^{-1} d_0} \quad (4)$$

4.4. Application of forward modeling

The modeling of ground acceleration in the six available stations was used to test the accuracy of two important pieces of information found with teleseismic data.

The teleseismic study of the Uttarkashi earthquake provides us two focal planes (NP1 and NP2). One of them is the plane containing the fault, so the first problem is to eliminate this ambiguity between those two nodal planes. Because of the effect of fault finiteness and directivity, the peak amplitude of strong motions contains information that allows us to discriminate between those two planes. We have computed forward models with the two focal mechanisms NP1 (strike 317°, dip 14°, slip 115°) and NP2 (strike 112°, dip 78°, slip 84°) found by the Centroid Moment Determination (CMT) of Harvard (Dziewonski et al., 1992). As already shown, this determination is more or less consistent with our long-period study (Table 2). The long-period study gives a rupture duration of 8 s. Since rupture velocities generally remain in the range of 0.8–0.95 of the shear wave speed in the source region, this source duration gives information about the source dimension, which is modeled as a simple planar fault 20 km long and 12 km wide (Fig. 4a). The slip chosen is uniformly distributed on the fault with a constant value of 3.0 m (this value of slip gives a moment of 1.6×10^{19} N m compatible with the moments determined from long-period studies) and the hypocenter has the location given by the India Meteorological Department (IMD). In Fig. 4b we compare the observed maxima with the results of the simulation for the two focal planes. The amplitude maxima of the synthetics obtained in this parameterization with NP2 show a clear disagreement with the data while the maxima found with NP1 are relatively close to the observations. In the following, NP1 is chosen to be the fault plane.

The epicentral determinations of the Uttarkashi earthquake, as reported by three different agencies are listed in Table 2. It is likely that the IMD solution which additionally used local short-period and regional data is the closest of the actual hypocenter. In the near field, the effect of fault finiteness and directivity can be quite important and the study of relative peak amplitude of ground motion at different strong-motion stations provides information about the direction of the rupture. Because of directivity, varying the hypocenter causes significant effects on ground acceleration in the near-field domain so that strong-motion data give an indication of the direction of the rupture propagation. Four different extreme models of rupture initiation at the far end of the fault are illustrated in Fig. 4a. In these forward models, the source was modeled as a simple planar fault (20 km long and 12 km wide) consistent with NP1. We chose a uniformly distributed slip on the fault with a constant value of 3.0 m. The maxima of the bandpassed (0.2–0.6 Hz) three-component accelerograms for the different models compared to the maxima of the bandpassed data are shown in Fig. 4c. Hypocenter 1 and a rupture propagation toward the west give the best agreement with the data. This hypocenter corresponds to the location of IMD and our modeling of the directivity effect confirms the accuracy of this determination.

In order to study the rupture process we need to know the absolute triggering time of each accelerogram. To solve this problem, the triggering time was computed by first matching by intercorrelation the first seconds of the observed waveforms with the first seconds of synthetic seismograms computed in a forward waveform model with a simple model (fault plane NP1, 20 km long and 12 km large, hypocenter

IMD, uniform slip 3 m, uniform rise time 2 s). This procedure gave us a first estimate of the absolute times.

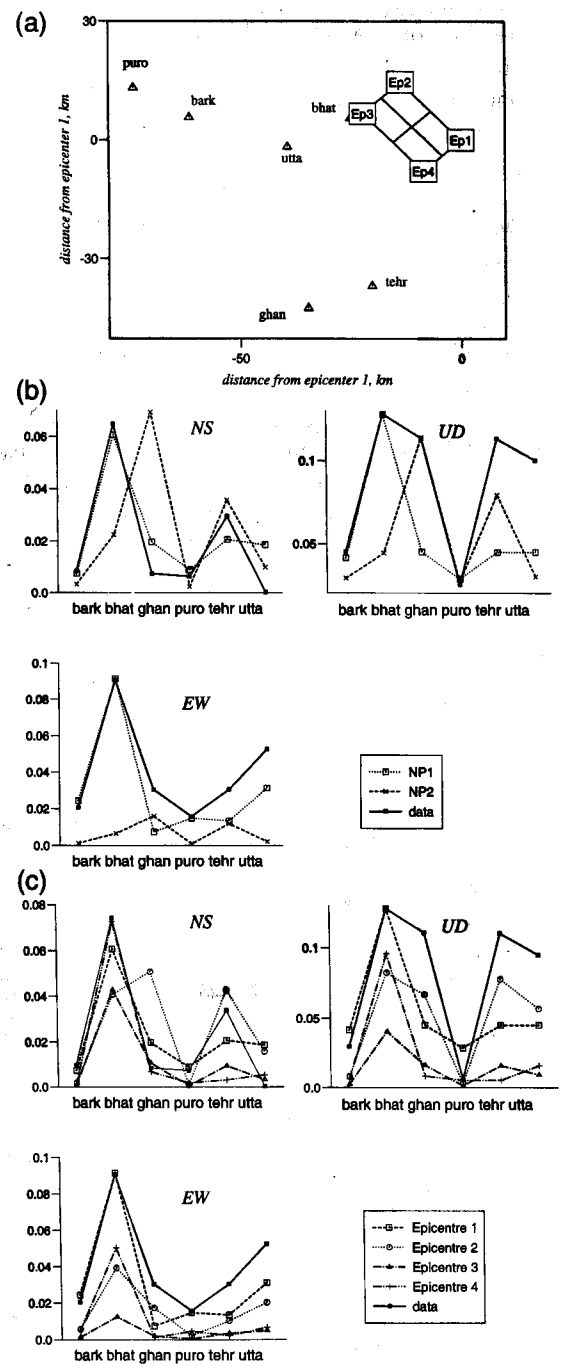

Fig. 4. (a) Location of the fault plane (NP1) and the hypocenters used in the forward modeling of the Uttarkashi earthquake. (b) Comparison of the data maxima of the bandpassed accelerograms (0.2–0.6 Hz) and the maxima of synthetics computed for the fault plane NP1 of the Harward CMT (Dziewonski et al., 1992) and different hypocenters. (c) Comparison of the data maxima of the bandpassed accelerogramms (0.2–0.6 Hz) and the maxima of synthetics computed for the two fault planes NP1 and NP2 of the Harward CMT (Dziewonski et al., 1992). For these two models the hypocenter is located in epicenter 1 of Fig. 4a (IMD localization).

4.5. Application of our inversion method to find the slip distribution

Our method operates through an iterative perturbation of the solution using locally determined gradients of the misfit surface. This method requires knowledge of an adequate starting solution. To chose this starting model we use some a priori information taken from seismotectonic studies and from our teleseismic inversion. The extreme limits of the rupture surface are estimated on the basis of the aftershocks and epicenter locations. According to this information we have chosen a fault plane of 48 by 36 km divided into 48 subfaults (6 km long by 6 km wide). Rupture velocities values generally remain in the range of 0.8–0.95 of the shear wave speed in the source region and we take the initial rupture velocity (2.7 km/s) to be 90% of the local shear wave speed in the source region. As already mentioned above, the source duration found by the teleseismic study is 8 s and it means that the fault surface defined by the 48 subfaults probably did not rupture entirely. In the starting model, a slip value of 0.2 m is prescribed on each subfault in the border of the fault. On the other subfaults, a value of 1.0 m is choosen. The seismic moment of this starting model is 1.2×10^{19} N m. The orientation of the fault plane and the focal mechanism on each subfault is given by NP1 of the Harvard CMT. The localization of the hypocenter is the localization given by IMD. This configuration is summarized in Fig. 5.

The observed and synthetic amplitude spectra at each station are equally normalized by the maximum observed amplitude spectra of the three components. This means that, for example, the weight given to each station in our inversion is independent of the

distance to the station. Indeed, the directivity effect and decay with distance remain present in our proposed physical model.

We assume that off-diagonal elements of C_d and C_p are equal to 0. The diagonal elements of C_d and C_p are given by the data and parameter variances. As mentioned by Hartzell (1989) the estimation of a priori variances in strong-motion inversion is not easy. We assume a value of 25.0 for the a priori variances of the rise time, the slip and the time of rupture of each subfault and a value of 2.0 for the data variance. Like Fukuyama and Irikura (1986), Fukuyama and Mikumo (1993) and Cotton and Campillo (1995) the diagonal values of C_p and C_d were found after several inversion tests to find the best convergence (with a constant of damping $b = 0.1$).

For each station, an inversion was first performed using only the data of this station. In this inversion the preliminary absolute times found by cross-correlation with a forward modeling were used. This inversion procedure with only one station shows the time at which the rupture had to begin on the subfault containing the hypocenter in order to match the first arrivals at that station. This time of the beginning of the rupture gave us the correction to apply to the preliminary absolute time. The other information given by this type of inversion (values of slip and rupture time on the other subfaults) are not useful. Such timing of accelerograms gives the possibility to account for hypocenter errors and to accomodate slight departures of the chosen velocity model from the actual crustal structure.

4.6. Influence of the choice of the starting model on the final solution: resolution study

The information taken from seismotectonic and teleseismic studies does not give any information on the possible values of the rise time. As noted by Hartzell and Mendoza (1991) or Cotton and Campillo (1994, 1995), dislocation rise time is one of the most difficult parameters to extract from the data. The consideration of this parameter has to take into ac-

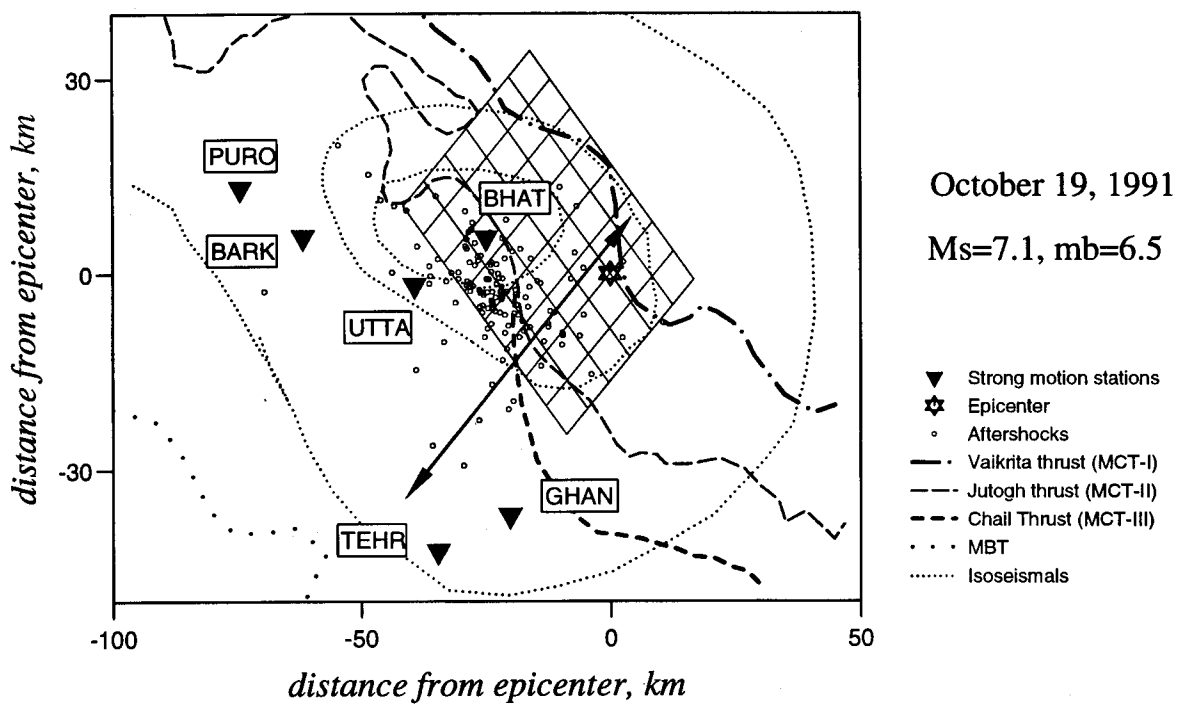

Fig. 5. Uttarkashi, Himalaya, India. Location map showing the fault plane (divided in 48 subfaults) used in the strong-motion inversion and the aftershocks of the Uttarkashi earthquake. The arrow shows the location of the cross section of Fig. 10.

count not only the fit to the data but also the value of the total moment. In order to specify the possible values of the rise time, we have performed a series of inversions with different values between 0.5 and 1.5 s. The different values lead to similar misfit but to significantly different seismic moment (Table 5). A simple explanation is the fact that the far-field seismic radiation is proportional to the derivative of the slip function. In spite of the complex configuration of the vicinity of an extended source, the dependence of the displacement on the slip velocity remains visible. Table 5 shows that a value of 1.0 s gives a good fit and an acceptable seismic moment. This value will be chosen in the inversion study described below.

Table 5
Misfit and moment deduced from the rupture models computed with different rise times

Rise time (s)	Variance reduction	Moment ($\times 10^{19}$ Nm)
0.5	0.43	1.02
1.0	0.42	1.55
1.5	0.35	2.0

Solutions of the strong-motion inversions can be divided into a stable and an unstable part (Olson and Apsel, 1982). The unstable part of the solution consists of distributions of slip which have little or no effect on the data. In other words, they are not resolved by these data. Since the inversion is not purely linear, the final values of the parameters which are not resolved by the data are mostly dependent on the a priori values chosen in the starting models. The trace (sum of the 96 diagonal elements) of the resolution matrix (Tarantola and Valette, 1982)

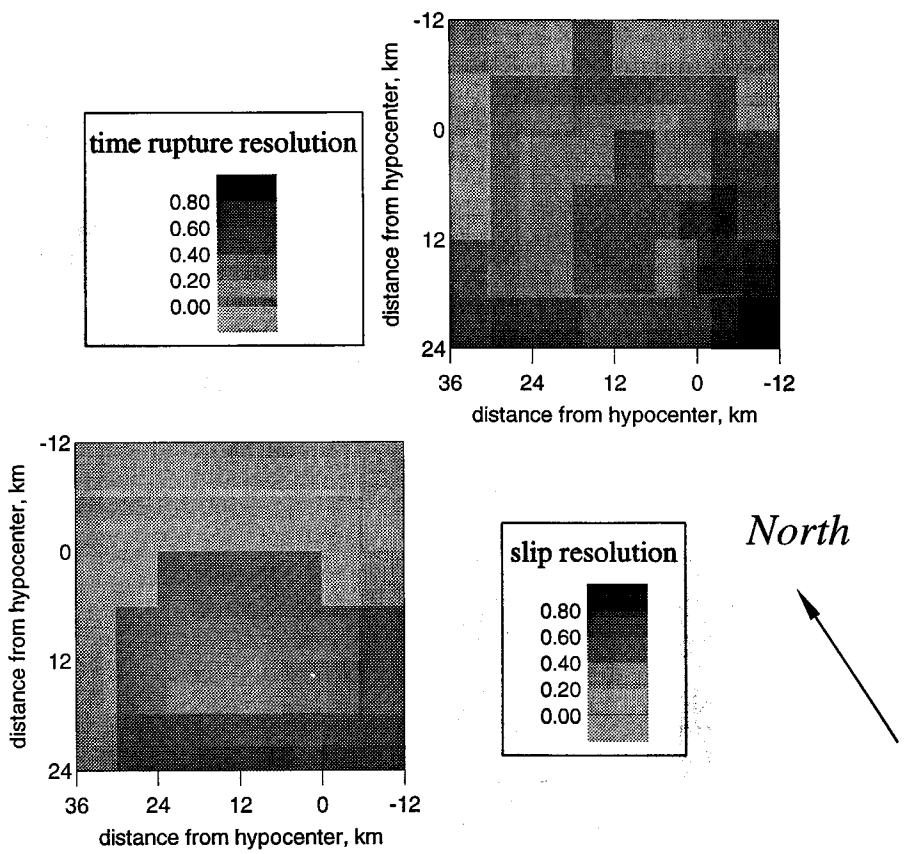

Fig. 6. Resolution matrix diagonal value calculated for each inverted parameter. Since these values depend on the choice of the a priori variance of each parameter, these maps are used for relative comparisons of the resolution in different parts of the fault.

indicates the number of parameters (49.3) that were effectively resolved by the data. This resolution information is lower for the slip (35%) than the rupture time (53%). The resolution maps of Fig. 6 give us an idea of the regions of the fault where our inversion is well constrained. These maps show us that the resolution is particularly bad in the northeastern part of the fault. This bad resolution in the northeastern part of the fault is explained by the absence of stations in this direction. Moreover, the stations are located southwest of the epicenter. Rupture on subfaults located northeast of the epicenter is then antidirective for the stations. Because of this directivity effect, even a large moment release in that region of the fault will not have a strong influence on the synthetic produced in the strong motions used in the inversion: the final slip distribution is then strongly dependent on the choice of the starting model in this region.

4.7. Results of the inversion

The synthetic waveform traces predicted by the slip distribution found by our inversion are compared with the observed seismic data in Fig. 7. Quantitative fit to the data using a measure of the variance reduction between the theoretical and recorded accelerograms for each station is given in Table 6. The mean variance reduction is 0.40. The two closer stations (Uttarkashi and Bhatwari) and the vertical components of all the stations show a good fit. On the other hand, horizontal components at the other stations are significantly lower than predicted. Yu et al. (1995) noticed that the velocity structure that worked for the two nearest stations and that we used in this inversion was not the best to predict the strong ground motion at more distant stations. Their trial-and-error modifications of the velocity model emphasize the potential role of unknown site and path effects, which could explain our poor fit of the horizontal components of distant stations.

The slip and rupture time distributions found by our inversion are shown in Fig. 8. The earthquake ruptured mainly to the southwest of the hypocenter for a distance of about 25 km; its total rupture duration is about 10 s. The slip distribution presents two maxima where slip is near 1.5 m: one is located 10 km west of the epicenter and occurred 4 s after the beginning of the rupture, the other one is located 15 km southwest of the epicenter and occcured about

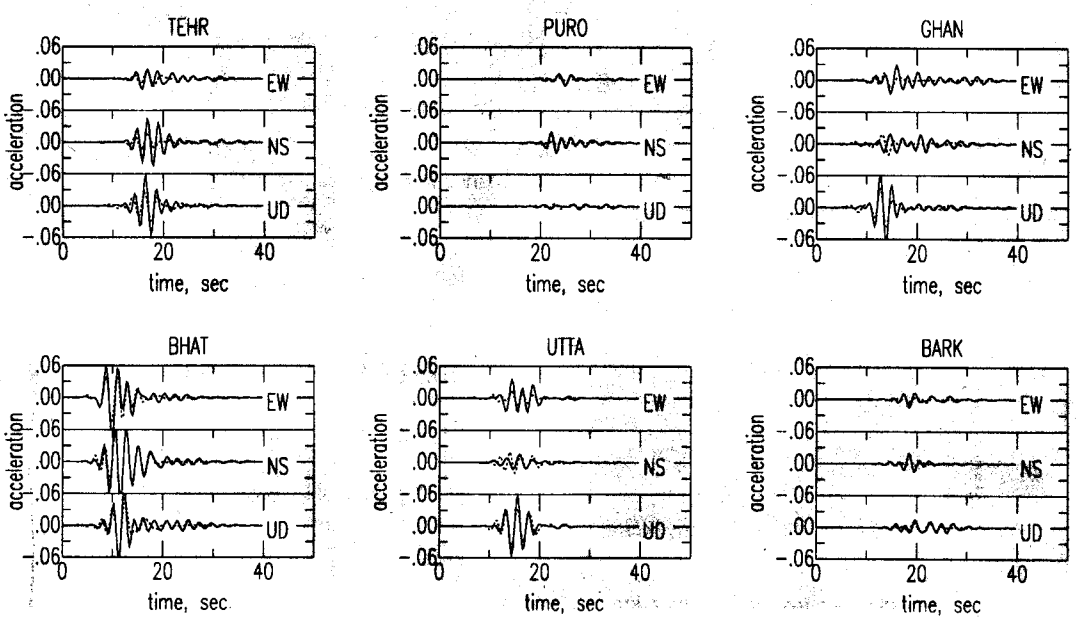

Fig. 7. Strong-motion accelerogram observations (solid lines) and synthetics (dashed lines) for the rupture model of Fig. 8. All have a common scale and have been band-passed in the same way (0.2–0.6 Hz).

Table 6
Variance reductions (a value of 1.0 means that the synthetic match perfectly the data)

	Bark	Bhat	Ghan	Puro	Tehr	Utta
N–S	0.04	0.90	−0.8	0.09	0.30	−0.30
E–W	0.31	0.78	0.21	0.20	0.12	0.49
U–D	0.43	0.67	0.70	−0.12	0.50	0.81

7 s after the beginning of the rupture. The total seismic moment of this rupture model is 1.5×10^{19} N m. This value is consistent with the values found from long-period teleseismic studies (Table 2). The final low slip distribution found through the inversion in the northeastern part of the fault is strongly dependent on the choice of the slip value in the starting model in that region. In other words, whatever the value of the slip in this region is, the fit to the strong-motion data will be the same. However, our model with no slip in that region gives a seismic moment which is in the range given by long-period studies. If more slip is added in this region, the moment infererred from our inversion will no more be in agreement with the one obtained from teleseismic records and CMT.

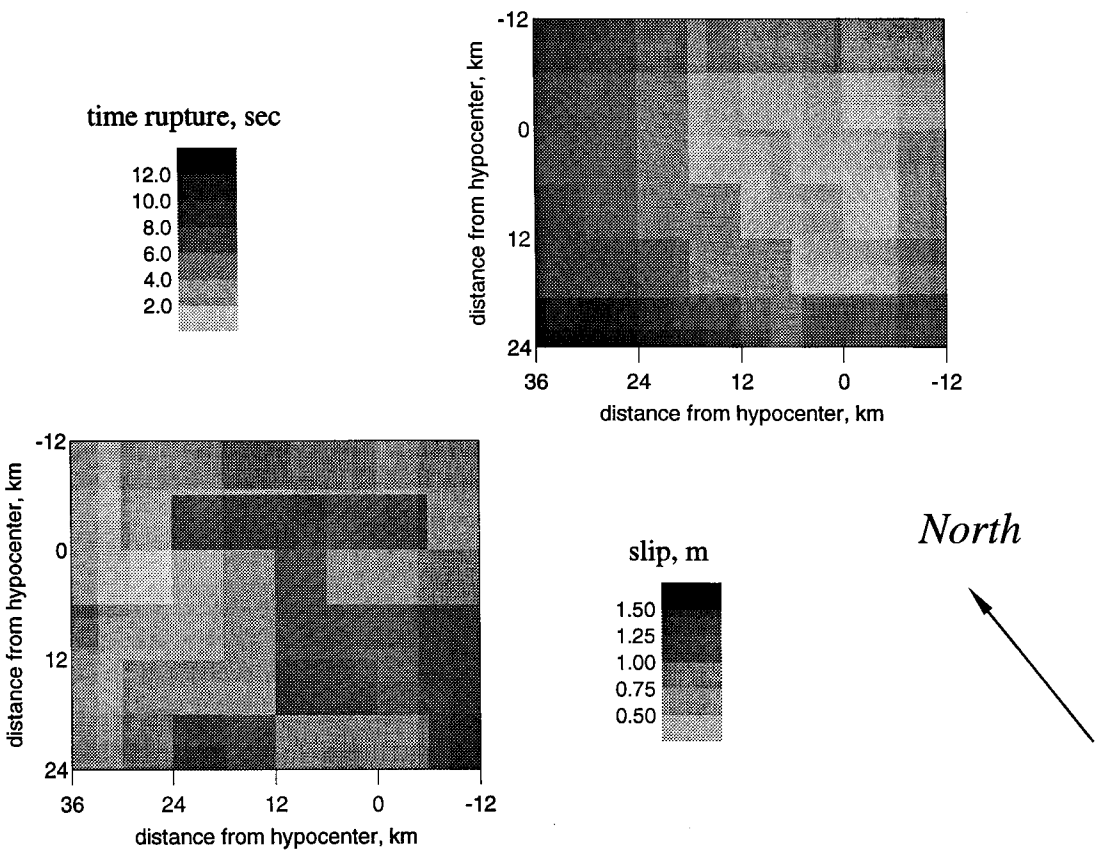

Fig. 8. Slip and rupture time distributions on the fault found by our strong-motion inversion. The seismic moment of this model is 1.5×10^{19} N m.

5. Discussion and conclusions

5.1. Source–time function

Because of the lack of absolute time, the imperfect azimuthal coverage and lack of knowledge of the structure, the set of strong-motion data used in this study is not ideal, and the resolution of our inversion is not as good as that of inversions recently performed with Californian earthquakes like the Landers earthquake of 1992 (Cohee and Beroza, 1994; Wald and Heaton, 1994; Cotton and Campillo, 1995). For this reason, we have tested the coherency of our strong-motion inversion with the work done with teleseismic data. The far-field source–time function obtained by integrating our inferred slip distribution across the fault and the source–time function found with our teleseismic study are shown in Fig. 9. Both inversions show that the Uttarkashi earthquake began with a small subevent. Most of the moment was released between 2 and 8 s of the rupture with a maximum rate of moment release about 4 s after the beginning of the rupture

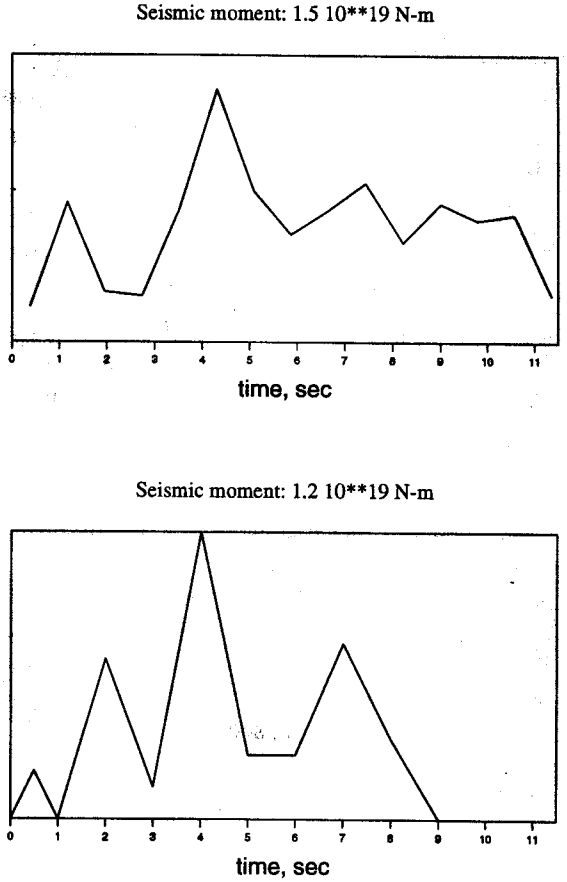

Fig. 9. Comparison of source time functions obtained from our point source analysis of teleseismic data (bottom) and our strong-motion inversion (top).

5.2. Spatial correlation of the rupture zone with aftershocks and isoseismals

The isoseismal map and the damage distribution observed in the field after the earthquake are described by Rastogi and Chadha (1994) and Kumar and Mahajan (1994). The region of most numerous aftershocks and the center of the damaged zone are located about 20 km west of the IMD hypocenter. This discrepancy between the localization of the hypocenter and the area of maximum damage was already noticed by Kayal et al. (1992) and Rastogi (1994). Our inversion study shows that the hypocenter area is not the zone of maximum slip. A zone of high moment release lies 15 km southwest of the hypocenter, which is closer to the center of the aftershocks and damage area. The observation of the aftershocks distribution (Fig. 5) shows that several aftershocks are not located on the fault zone but a little more southward. It is possible that aftershock distribution does not define the area where slip occurred during the earthquake, but rather defines the zones where rupture stopped. This conclusion was already reached for Californian earthquakes (Mendoza and Hartzell, 1989; Hartzell and Iida, 1990). This effect is expected since it was shown that, in the case of a crack, stresses increase at the edges of the rupture area (Das and Sholz, 1982).

5.3. Tectonic interpretation

The Uttarkashi earthquake provides information on the tectonic processes currently affecting the Garhwal province. In this region, various sedimentary and metamorphic units are repeated several times as a results of imbricated thrusting along faults like the Jutogh and the Chail thrusts (Valdiya, 1980). This earthquake is not the result of slip along on one of these imbricate thrusts, but rather it ruptured a low-angle thrust fault that extends south of the

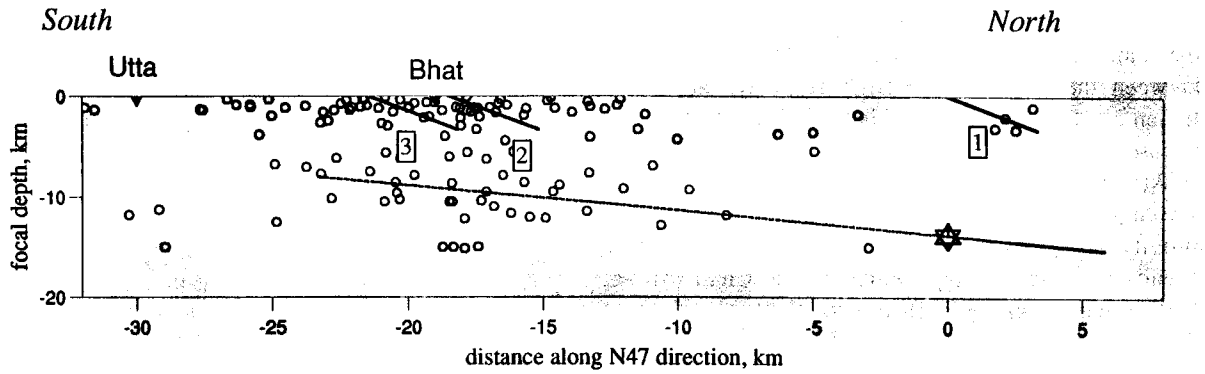

Fig. 10. Cross section across the Uttarkashi region showing the fault plane (dashed line) and the epicenter (star) used in this study and the main thrusts mapped on the field. *1* = Vaikrita thrust; *2* = Jutogh thrust; *3* = Chail thrust. Aftershocks of the Uttarkashi earthquake are also plotted alongside the cross section (○).

Vaikrita thrust. Microearthquake monitoring during 1979–1980 and 1984–1986 indicated a concentration of the seismicity north of Uttarkashi (Khattri et al., 1989). The majority of the 252 earthquake epicenters determined with this array lie close to or south of the surface projection of the MCT-II (Fig. 1) with depth less than 10 km. A cross section of the Uttarkashi region showing the fault plane of the earthquake, the location of the aftershocks and the fault trace of the main thrusts near the surface is presented in Fig. 10.

We propose in Fig. 11 an interpretative cross

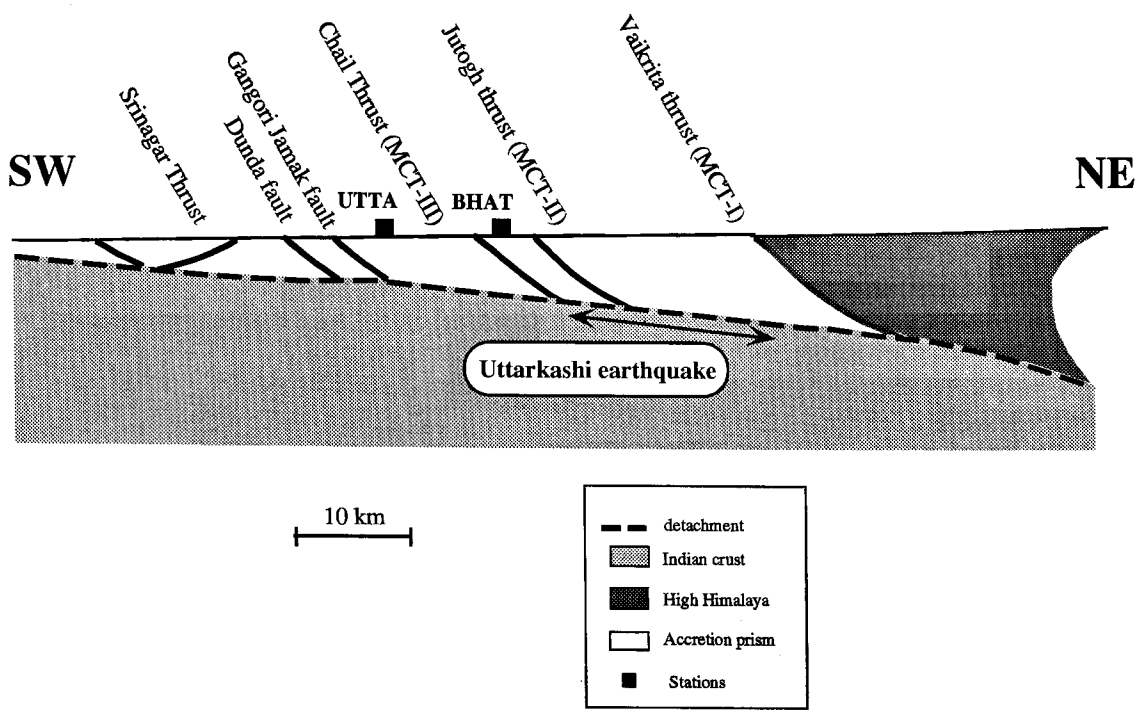

Fig. 11. Interpretative cross section showing our tectonic interpretation of the Uttarkashi region and the localization of the earthquake in this tectonic scheme. Note: Accretion prism should read Crustal accretion prism.

section of the Uttarkashi region: the region south of the Vaikrita thrust forms a crustal accretion prism between the block of the High Himalaya and the Indian crust. At the base of this wedge, a detachment releases strain energy in moderate to large earthquakes such as the Uttarkashi earthquake. Between two major events on the detachment, the seismic activity is weak: aftershocks and microseismicity occur on the surounding faults like the Chail (MCTIII) of the Jutogh (MCTII) thrusts. Farther north the detachment fault probably steepens beneath the Higher Himalaya and become aseismic. As proposed recently by Pandey et al. (1995), large Himalayan earthquakes could nucleate there. In this region, the greatest seismic hazard is then from these large detachment earthquakes and one important point question is the location of the northern limits of the seismic part of the detachment. Our study of the Uttarkashi earthquake shows that this earthquake occurred north of the Jutogh (MCTII) and south of Vaikrita thrust (MCTI). The region on the detachment where big earthquakes can develop extends in the north at least to the Vaikrita thrust. This conclusion is important for correctly estimating the seismic hazard in the Uttarkashi region.

Acknowledgements

We thank R. Madariaga and two anonymous reviewers for their comments and suggestions that have inproved this version. We have also benefited from useful discussions with P. Lefort and J.P. Avouac. This project has been supported by project Mecalith (INSU/CNRS). The authors are grateful to Prof. A.R. Chandrasekaran for providing the digitized acceleration data. The work was started during the visit of B.K. Rastogi to Grenoble in 1993 under the European Council Department of Science and Technology Programme.

References

Argand, E., 1924. La tectonique de l' Asie. Int. Geol. Congr. Rep. Sess., 13: 170–372.

Beroza, G.C. and Spudich, P., 1988. Linearized inversion for fault rupture behavior: Application to the 1984 Morgan Hill, California, earthquake. J. Geophys. Res., 93: 6275–6296.

Bouchon, M., 1981. A simple method to calculate Green's function for layered media. Bull. Seismol. Soc. Am., 71: 959–971.

Campos, J., Madariaga, R., Nábèlek, J., Bukchin, B.G. and Deschamps, A., 1994. Faulting process of the 1990 June 20 Iran earthquake from broadband records. Geophys. J. Int., 118: 31–46.

Chandra, U., 1978. Seismicity, earthquake mecanism and tectonics along the Himalayan mountain range and vicinity. Phys. Earth Planet. Inter., 16: 109–131.

Chandrasekaran, A.R. and Das, J.S., 1992. Analysis of strong motions accelerograms of Uttarkashi Earthquake of October 20, 1991. Bull. Indian Soc. Earth Technol., 29(1): 35–55.

Cohee, B.P. and Beroza, G.C., 1994. Slip distribution of the 1992 Landers earthquake and its implications for earthquake source mechanism. Bull. Seismol. Soc. Am., 84: 692–712.

Cotton, F. and Campillo, M., 1994. Application of seismogram synthetis to the study of earthquake source from strong motion records. Ann. Geofis., 37: 1539–1564.

Cotton, F. and Campillo, M., 1995. Frequency domain inversion of strong motions: application to the 1992 Landers earthquake. J. Geophys. Res., 100: 3961–3975.

Das, S. and Sholz, K., 1982. Off fault aftershock clusters caused by shear stress increase? Bull. Seismol. Soc. Am., 71: 1669–1675.

Dziewonski, A.M., Ekström, G. and Salganik, M.P., 1992. Centroid-moment tensor solutions for October–December 1991. Phys. Earth Planet. Inter., 74: 89–100.

Fukuyama, E. and Irikura, K., 1986. Rupture process of the 1983 Japan Sea earthquake using a waveform inversion method. Bull. Seismol. Soc. Am., 76: 1623–1640.

Fukuyama, E. and Mikumo, T., 1993. Dynamic rupture analysis: inversion for the source process of the 1990, Japan, earthquake. J. Geophys. Res., 98: 6529–6542.

Gansser, A., 1964. Geology of the Himalaya. Interscience, New York, NY, 298 pp..

Hartzell, S.H., 1989. Comparison of seismic waveform results for the rupture history of a finite fault: Application to the 1896 North Palm Springs, California, earthquake. Bull. Seismol. Soc. Am., 94: 7515–7534.

Hartzell, S.H. and Mendoza, C., 1991. Application of an iterative least-squares waveform inversion of strong-motion and teleseismic records to the 1978 Tabas, Iran, earthquake. Bull. Seismol. Soc. Am., 81: 305–331.

Hartzell, S.H. and Heaton, T.H., 1983. Inversion of strong ground motion and teleseismic waveform data for the fault rupture history of the 1979 Imperial Valley, California, earthquake. Bull. Seismol. Soc. Am., 73: 1553–1583.

Hartzell, S.H. and Iida, M., 1990. Source complexity of the 1987 Whittier Narrows, California, earthquake from the inversion of strong motion records. J. Geophys. Res., 95: 12,475–12,485.

Kayal, J.R., Kamble, V.P. and Rastogi, B.K., 1992. Aftershocks sequence of Uttarkashi earthquake of October 20, 1991. Geol. Surv. India, Spec. Publ., 30: 203–217.

Kennett, B.L.N., 1983. Seismic Wave Propagation in Stratified Media. Cambridge Univ. Press, New York, NY.

Khattri, K.N., 1987. Great earthquakes, seismicity gaps and poten-

tial for earthquake disaster along the Himalaya plate boundary. Tectonophysics, 138: 79–92.

Khattri, K.N., 1992. Local seismic investigations in the Garhwal–Kumaon Himalaya. Mem. Geol. Soc. India, 23: 275–302.

Khattri, K.N., Chander, R., Gaur, V.K., Sarkar, I. and Kumar, S., 1989. New seismological results on the tectonics of the Garhwal Himalaya. Proc. Indian Acad. Sci. Earth Planet., 98: 91–109.

Kumar, S. and Mahajan, A.K., 1994. The Uttarkashi earthquake of 20 October 1991: field observations. Terra Nova, 6: 95–99.

LeFort, P., 1975. Himalayas: the collided range. Present knowledge of the continental arc. Am. J. Sci., 245-A: 1–44.

Lyon-Caen, H. and Molnar, P., 1983. Constraints on the structure of the Himalayas from an analysis of gravity anomalies and a flexural model of lithosphere. J. Geophys. Res., 88: 8171–8191.

Mendoza, C. and Hartzell, S.H., 1989. Slip distribution of the 19 September 1985 Michoacan Mexico earthquake: Near source and teleseismic constraints. Bull. Seismol. Soc. Am., 79: 655–669.

Mendoza, C., Hartzell, S.H. and Monfrey, T., 1994. Wide-band analysis of the 3 March 1985 Central Chili earthquake: overall source process and rupture history. Bull. Seismol. Soc. Am., 84: 269–283.

Molnar, P. and Tapponier, P., 1975. Tectonics of Asia: Consequences and implication of a continental collision. Science, 189: 419–426.

Molnar, P., Fitch, T.J. and Wu, F.T., 1973. Fault plane solutions of shallow earthquakes and contempary tectonics in Asia. Earth Planet. Sci. Lett., 19: 101–112.

Nábèlek, J.L., 1984. Determination of earthquake source parameters from inversion of body waves. Ph.D. Thesis, MIT, Cambridge, MA.

Nábèlek, J.L., 1985. Geometry and mechanism of faulting of the 1980 el Asnam, Algeria, earthquake from inversion of teleseismic waves and comprison with field observations. J. Geophys. Res., 90: 12,713–12,728.

Ni, J. and Baranzangi, M., 1984. Seismotectonics of the himalayan collision zone: geometry of the underthrusting indian plate beneath the Himalaya. J. Geophys. Res., 89: 1147–1163.

Olson, A.H. and Anderson, J.G., 1988. Implications of frequency-domain inversion of earthquake ground motion for resolving the space–time dependence of slip on an extended fault. Geophys. J., 94: 443–455.

Olson, A.H. and Apsel, R.J., 1982. Finite fault and inverse theory with applications to the 1979 Imperial Valley earthquake. Bull. Seismol. Soc. Am., 72: 1969–2001.

Pandey, M.R., Tandukar, R.P., Avouac, J.P., Lavé, J. and Massot, J.P., 1995. Interseismic strain accumulation of the Himalayan crustal ramp (Nepal). Geophys. Res. Lett., 751–754.

Rastogi, B.K., 1994. Seismological studies of Uttarkashi earthquake of October 20, 1991. J. Geol. Soc. India.

Rastogi, B.K. and Chadha, R.K., 1994. Intensity and isoseismals of Uttarkashi earthquake of October 20, 1991. J. Geol. Soc. India.

Seeber, L., Armbruster, J. and Quittmeyer, R., 1981. Seismicity and continental subduction in the Himalayan arc. In: H.K.G. and F.M. Delany (Editors), Hindu Kush, Himalaya: Geodynamic Evolution. Zagros. Am. Geophys. Union, Geodyn. Ser.

Smith, L.R.B., 1843. Memoir on India earthquakes. J. Asiat. Soc. Bengal., 12: 1029–1059.

Takeo, M., 1987. An inversion method to analyse the rupture processes of earthquakes using near-field seismograms. Bull. Seismol. Soc. Am., 77: 490–513.

Tapponnier, P. and Molnar, P., 1977. Active faulting and Cenezoic tectonics in China. J. Geophys. Res., 82: 2945–2969.

Tarantola, A., 1987. Inverse Problem Theory. Elsevier, Amsterdam–Oxford–New York–Tokyo.

Tarantola, A. and Valette, B., 1982. Generalized nonlinear inverse problem solved using the least squares criterion. Rev. Geophys. Space Phys., 20: 219–232.

Valdiya, K.S., 1980. The two intracrustal boundary thrusts of the Himalaya. Tectonophysics, 66: 323–348.

Wald, D.J. and Heaton, T.H., 1994. Spatial and temporal distribution of slip for the 1992 Landers, California, earthquake. Bull. Seismol. Soc. Am., 84: 668–691.

Yu, G., Khattri, K.N., Anderson, J.G., Brune, J.N. and Zeng, Y., 1995. Strong ground motion from the Uttarkashi earthquake: comparison of observations with synthetics using the composite source model. Bull. Seismol. Soc. Am., 85: 31–50.